DOI: 10.1002/((adma.201802290))
Article type: Communication

Photosynthetic Bioelectronic Sensors for Touch Perception, UV-Detection and Nanopower Generation: Toward self-powered e-skins

*Sai Kishore Ravi, Tingfeng Wu, Vishnu Saran Udayagiri, Xuan Minh Vu, Yanan Wang, Michael R. Jones, Swee Ching Tan**

S. K. Ravi, T. Wu, V. S. Udayagiri, X. M. Vu, Y. Wang, Prof. S. C. Tan

Department of Materials Science and Engineering, National University of Singapore, 9 Engineering Drive 1, Singapore 117575

E-mail: msetansc@nus.edu.sg

Dr. M. R. Jones

School of Biochemistry, University of Bristol, Biomedical Sciences Building, University Walk, Bristol BS8 1TD, United Kingdom.

Keywords: Polysensory e-skin, Tactile sensing, Electronic skin, Flexible electronics, Photosynthetic proteins, Nanopower generation, Energy self-sufficiency

Abstract:

Energy self-sufficiency is an inspirational design feature of biological systems that fulfill sensory functions. Plants such as 'touch-me-not' (*Mimosa pudica*) and 'Venus flytrap' (*Dionaea muscipula*) not only sustain life by photosynthesis but also execute specialized sensory responses to touch. Photosynthesis enables these organisms to sustainably harvest and expend energy, powering their sensory abilities. Photosynthesis therefore provides a promising model for self-powered sensory devices such as electronic skins (e-skins). While the natural sensory abilities of human skin have been emulated in man-made materials for advanced prosthetics and soft-robotics, no previous e-skin has incorporated phototransduction and photosensory functions that could extend the sensory abilities of human skin. Here we present a proof-of-concept bioelectronic device integrated with natural photosynthetic pigment-proteins that not only shows an ability to sense touch stimuli (down to 3000 Pa) but also to

sense low-intensity UV radiation (down to 0.01 mW/cm^2) and generate an electrical power of ≈260 nW/cm^2. The scalability of this photoprotein-based sensing device is demonstrated through the fabrication of flexible, multi-pixel bioelectronic sensors capable of touch registration and tracking. The polysensory abilities, energy self-sufficiency and additional nanopower generation exhibited by this bioelectronic material make it particularly promising for applications such as smart e-skins and wearable sensors, where the photo-generated power can enable remote data transmission.

Introduction:

Central to our ability to detect and evaluate the myriad objects we come into direct contact with daily is the sense of touch enabled by human skin[1-5]. Tactile sensing is a common attribute among animals, but responses to mechanical stimuli can be varied. In humans, for example, the response to a touch can be physiological or psychological in addition to physical. It is known that tactile sensing by skin is facilitated by receptors and sensory neurons[1, 4, 5], and the mechanisms through which stimuli are detected by the receptors and the information distributed by neurons are active areas of research[6]. These receptors enable sensitivity to varied pressure, vibration, strain, temperature and humidity stimuli that includes recognition of irritation and pain[1, 7]. The skins of some animals exhibit attributes not displayed by humans, including the well-known capabilities for camouflage and communication through environmentally-triggered colour changes most commonly associated with chameleons[8] and cephalopods[9].

An appealing attribute of the sensory abilities of biological systems is that they are powered by energy autonomously harvested from ambient sources without the need of any persistent external power supply such as is necessary for man-made electronic sensors. Sensory functions in certain plants such as “touch-me-not” (*Mimosa pudica*) are particularly inspirational as models for electronic sensors as they exhibit energy self-sufficiency, their sensory abilities being sustained by just by a fraction of the energy harvested by photosynthesis. While attempts

have been made to mimic the complex biological sensory systems of the human skin in synthetic electronic skins, the rationale of the work reported here is to look at how photosynthesis can be used to enhance the sensory abilities of an electronic skin and make it self-contained in terms of the energy required for its sensory functions.

Synthetic electronic skins are being developed for a variety of potential applications including biomimetic prosthetics, soft robotics, health monitoring, energy harvesting and enhanced sensing[1, 5, 10-16]. A fundamental goal is emulation of the tactile sensing function of natural skins in electronic devices[17-25]. Tactile sensing has been implemented through a variety of working principles in touch screen technologies and artificially intelligent systems including electronic skins[17-22, 26], with resistive and capacitive sensors being the most commonly employed components in commercial touch screens. Resistive sensors comprise two parallel conductors separated by spacer pads, touch being sensed by a change in resistance at a local point where the two conductors are brought into contact[26-28]. In a resistive-touch mobile phones, as a stylus is used to apply a pressure at a point, the two electrodes come in contact essentially completing the circuit at that point which aids in locating which part of the touch panel is triggered. Capacitive touch panels typically consist of a glass sheet coated with a transparent conductive film which, when touched by a conductor (e.g. a human finger), experiences an electrostatic field distortion that is detected as a change in capacitance[26]. Alternative sensing mechanisms such as piezoresistivity[29], piezoelectricity[30, 31], piezotronics[32-34], triboelectricity[13, 35, 36], tribotronics[26] and field-effect transistors[19] have also been employed in materials fabricated to mimic biological skin. Many of these approaches require the sensing material to be connected to a continuous or rechargeable power source to provide a practical sensing function, and so there is also interest in development of solar cells, energy harvesters and batteries that can be incorporated into electronic skins[10, 11, 37, 38]. The engineering of self-powered electronic systems is also of great interest[39], and approaches to the development of self-powered electronic systems for sensor applications have been described in comprehensive reviews[40-42].

Mimicry of the multiple and diverse sensory abilities of animal skins presents considerable challenges. Many recent reports have either focused on improving the sensitivity of an electronic skin to a mechanical or thermal stimulus, or have been aimed at developing a more versatile electronic skin by increasing the number of sensory abilities it displays. As an example of the former an ultra-sensitive piezo-resistive electronic skin has been reported that is able to detect pressures lower than 1 Pa[18]. A noteworthy example of the latter is a description of a stretchable prosthetic skin based on silicon nanoribbon electronics that can sense pressure, temperature, strain and humidity[43]. Electronic skins that mimic the optical properties of chameleon and cephalopod skins have also been attempted [8, 9, 11, 44].

In addition to its pressure and temperature sensing attributes, human skin displays a complex set of responses to natural sunlight and artificial light sources[28]. It is known that the exposure of skin to UV radiation can cause DNA damage and skin cancer[45-47], and UV exposure also contributes to compositional and morphological changes associated with skin ageing[48]. The development of electronic skins with light sensing and/or photoprotective functions is of particular relevance to skin prostheses and wearable materials for health monitoring, most obviously where exposure to UV or strong visible light needs to be avoided.

In addition to the need to widen the sensory abilities of electronic skins for prosthetics and wearable electronic systems, to realize practical systems for daily use, the development of energy self-sufficiency in electronic skins has become highly desireable. Autonomous functioning of electronic skins without any continuous power supply has hence become an important challenge. Taking inspiration from the energy management and self-sufficiency achieved in sensory plants, where solar energy harvesting not only powers tactile sensing and light sensing functions but also a plethora of other biological functions, the present work demonstrates the rationale of engineering future electronic skins that are not only energetically self-contained but also generate surplus power that could be expended on allied electronic functions. The objective of the present work was to explore the development of a self-powering

bioelectronic system that is sensitive to touch and has additional light-responsive functions that can warn of excessive levels of harmful solar UV radiation. The flexible sensor we describe here is based on a photosynthetic protein that has multiple absorbance bands that span the biologically-relevant wavelengths of the solar spectrum. The properties of this natural, environmentally benign and biodegradable photovoltaic pigment-protein enabled three functionalities, power generation, touch sensing and UV detection, in a flexible bioelectronic device for prospective e-skin applications.

Results and Discussion:

The bioelectronic device was assembled from a flexible top electrode comprising an indium tin oxide coated polyethylene terephthalate film (ITO-PET) which is a commonly used electrode in flexible electronics[17, 23], a blend of photosynthetic protein and electron transfer mediator, and a flexible base electrode comprising a gold-coated PET film (**Figure 1a**). The photosynthetic protein was the *Rhodobacter sphaeroides* RC-LH1 reaction centre/light harvesting complex (**Figure S1**), which has multiple absorbance bands between 200 and 950 nm (**Figure 1b**). The mediator was 100 mM ubiquinone-0 (Q0) dispersed in a gel matrix formed from succinonitrile (SCN) and water. Solutions of concentrated protein (100 µM) and Q0-SCN were mixed in a 5:1 ratio (v/v) to form a two-phase system (**Figure 1a**). The resulting composite material was transparent across the visible spectrum with a maximum transmittance of ≈50 % between 520 nm and 550 nm (**Figure 1c**). The decline in transmittance below 500 nm in **Figure 1c** is attributable to the carotenoids of the RC-LH1 complex that absorb between 400 and 500 nm (**Figure 1b**). The dip in transmittance at 590 nm in **Figure 1c** is due to a minor absorbance band of the bacteriochlorophylls, the main absorbance of which lies outside the visible with major bands peaking at 376 nm and 874 nm (**Figure 1b**). The absorbance of the protein around 275 nm (**Figure 1b**) is attributable to aromatic amino acids, principally tryptophan.

The two-phase RC-LH1/Q0-SCN formulation enabled the material to not only function as a bio-photoelectrochemical cell[49, 50] (see below) but also as an electrochemical capacitor. Cells assembled in ambient light displayed a built-in potential difference of -530 mV to -600 mV between the two electrodes. We attribute this to electrochemical interactions between the electrodes and the cell contents, with the possibility of contributions from photoactivity of the RC-LH1 protein. Photoexcitation is expected to initiate trans-protein charge separation within the RC-LH1 complex, forming a cation on a pair of bacteriochlorophyll molecules at one terminal of the protein (P^+) and an anion on a quinone at the opposite terminal (Q_B^-) (**Figure 1d**, and see Supplementary **Figure 1**). Consistent with their vacuum potentials, the ITO electrode was capable of direct electron transfer to adjacent P^+ sites, whilst the Au base electrode was able to accept electrons either directly from Q_B^- or, after electron transfer across the heterojunction, from the Q0 entrapped in the SCN plastic crystalline phase (**Figure 1d**). In the protein/Q0-SCN blend the high capacitance of the protein-only phase was offset by the moderate conductance of the Q0-SCN phase. The use of SCN, a plastic crystalline material with a high dielectric constant ($\kappa = 55$ at room temperature), aided in the build-up of the potential difference of the cell. SCN has been used previously in electrochemical double layer capacitors[51] but to the best of our knowledge has not been used for an electronic skin.

Touch sensing was based on modulation of this base voltage difference (V_{OC}). The application of pressure brought the electrodes into contact at the point of touch, resulting in a localized low-resistance path for electron flow in the device that reduced the V_{OC} to zero (**Figure 2a-c**). The tactile sensing capability of the material was tested by applying either instantaneous or continuous loads to an area of 0.6 cm^2. For both types of load no response was observed below 0.2 N of applied force, but an average voltage response of 0.65 mV was seen between 0.2 N to 0.4 N (**Figure 2d**). This voltage shift was constant during an applied load. A 0.5 N load produced a larger average voltage shift of 24 mV that relaxed to the pre-load level over ~15 seconds (**Figure 2e**), and progressively higher instantaneous loads in the range 0.6-1.0 N

produced progressively greater initial voltage changes that relaxed over ~100 seconds. As the instantaneous load was increased to 1 N, the measured voltage shifted to 0 V (**Figure 2e**). To confirm the formation of a low-resistance path under an applied load, I-V curves were recorded by cyclic voltammetry under continuous-load and no-load conditions. In contrast to the no-load condition (**Figure 2f**, blue), under a 1 N load a high current was obtained at all non-zero applied voltages and the I-V curve became a straight line indicating ohmic behavior (**Figure 2f** and inset).

A plot of the initial voltage shift as a function of instantaneously applied pressure revealed three response regimes (**Figure 2g**). The material could sense pressures as low as 3000 Pa, which lies within the low-pressure regime typical of a sensation such as a gentle finger touch (1000 to 10000 Pa), with a graded response between ~7000 and 10000 Pa. There was also a high voltage response of up to 600 mV in the medium-pressure regime above 10000 Pa.

The voltage response to applied pressure was relatively rapid, highly reproducible and was only seen when the photosynthetic protein was included in the material (**Figure 3a**). In addition to supporting a much higher base voltage the protein/Q0-SCN blend was largely liquid and deformable in contrast to a pure Q0-SCN phase which was gel-like and non-deformable. Under a ~1.0 s load of 1 N the shift to 0 V was complete within ~0.5 s and, if reapplied in a cyclical fashion, this zero V_{OC} was restored in a few tenths of a second (**Figure 3a**). Applying instantaneous force at a fixed frequency allowed the V_{OC} to be oscillated between selected values in a highly reproducible fashion over different time scales; e.g. between 0 and -0.15 V utilizing partial relaxation of the touch response (**Figure 3b**) or between 0 and -0.57 V utilizing near full relaxation over a longer period (**Figure 3c**). The graded responses could be used for different purposes if integrated into an electronic device; for an application requiring a short response time a voltage transient of 0.1 V is high enough to be detected by a micro/macro sensor.

In addition to touch sensing, the bioelectronic system exhibited a capability for solar energy conversion. Under white light illumination (one sun; 100 mW/cm^2) the material generated a

photocurrent density of ≈1.1 μA/cm^2 (**Figure 4a**) and a photovoltage of 0.25 V (**Figure 4b**). This corresponded to a power density of ≈260 nW/cm^2 which is sufficient to drive a low-power electronic system. The mechanism of photocurrent generation is summarized in **Figure 1d** and **Figure S1**. It is worthwhile to note that incident light enabled generation of surplus electric power as the device serves also as a photo-electrochemical cell. However, the touch sensing was independent of illumination, the voltage signal being due to the change in base potential when a low resistance path is created in the cell in response to the applied pressure.

The UV absorbance of the RC-LH1 complex enabled a third functionality for the bioelectronic device, the bands centred at 275 nm and 376 nm corresponding to the regions classified as UV B (280-315 nm) and UV A (315-400 nm). UV A is the most penetrating, and is associated with skin wrinkling and aging, whilst UV B is associated with sunburn[52]. Both are causative agents of skin cancer through a variety of mechanisms, with particular concern over the link between UV B and malignant melanoma[53]. With illumination centred at 254 nm a photoresponse was seen to intensities as low as 0.01 mW/cm^2 (**Figure 4c**) despite the fact that only 10 % of the incident light reached the RC-LH1 proteins due to low transmittance of the ITO-PET electrode at this wavelength. Similar sensitivity was seen with UV light centred at 365 nm (**Figure 4d**), and application of this over a wider range showed that the peak photoresponse scaled with intensity (**Figure S2**). Excitation light centred 365 nm light excites the bacteriochlorophyll "Soret" band at 376 nm (**Figure 1b**), producing the first singlet excited state of the P bacteriochlorophylls in the RC through a combination of internal conversion and energy transfer, and so initiating a photocurrent. Light centred at 254 nm would be expected to excite the aromatic amino acids that give rise to the band at 275 nm, the observed photocurrent being attributable to Förster resonance energy transfer into the bacteriochlorophyll Soret absorbance band followed by normal charge separation[54]. The high sensitivity of the photosynthetic proteins to incident UV radiation of different wavelengths is promising for development of a

more sophisticated electronic skin capable of alerting the user to the type and intensity of incident UV radiation.

Attributes of the tactile sensing functionality of the material were demonstrated using an electronic circuit interface (**Figure S3**) to translate touch responses into an LED readout. As the touch response was based on electrical/electrochemical changes within the material, and not on any change in surface property such as temperature or electrical charge, it could be triggered with styluses made of any material (not shown) and a touch response could also be registered under water (**Figure S4, movie S1**). The touch response could also be demonstrated in the dark, emphasizing that it was not light-dependent (**movie S2**).

The material could also be scaled to form a 3-pixel and 9-pixel touch sensor through a simple fabrication scheme. To fabricate a 9-pixel sensor the Au electrode was patterned with nine active areas each of which had a distinct terminal (**Figure 5a**), whilst the ITO electrode was patterned with nine active areas that were connected to form a single terminal (**Figure 5b**). A continuous film of protein/Q0-SCN blend was then introduced between the two electrodes, which were separated by a spacer around the periphery (**Figure 5c**, red), to form a sandwich structure with pixels aligned (**Figure 5d and 5e**). The touch-induced voltage change was used to register the spot touched (**Figure 5f**) and to continuously track the position of the touch, functionalities that are both crucial for integration of an electronic skin into soft robotics.

The touch responses of the 3- and 9-pixel cells were demonstrated by connecting them to an array of LEDs by an electronic interface (**Figure S3**). Touch registration and tracking were demonstrated with a 3-pixel cell in a planar conformation (**Figure 6a, movies S3, S4**) and could also be obtained when the cell was in a flexed conformation (**Figure 6b, movies S5, S6**). Multidirectional touch tracking could be demonstrated using the 9-pixel cell (**Figure 7, movie S7**). Unlike microfluidic tactile sensors[55-57] that need fluid to be contained in discrete small areas, which makes scaling up expensive, the present model presents an economic alternative in which the protein/Q_0-SCN blend was not confined to individual pixels but rather formed a

continuous phase between pixelated flexible electrodes. More detailed notes on the UV sensing and the touch sensing functions and the respective demonstrations can be found in the Supporting Information.

To conclude, we have engineered a proof-of-concept bioelectronic sensor based on a natural photosynthetic protein. In addition to being able to convert solar energy into DC electrical power the material is potentially capable of discriminatory UV sensing and touch sensing. To our knowledge, this is the first report of a material/system that displays this combination of functionalities. Although the power density generated by the sensor is modest it is sufficient to drive a low power electronic system. Such inbuilt functionality is particularly relevant to future prosthetic skins for health monitoring, where the power generated could be used to transmit collected sensory data to a receiver by low-power wireless electronics.

Supporting Information
Supporting Information is available from the Wiley Online Library or from the author.

Acknowledgements
S.C.T. acknowledges the financial support from MOE AcRF 1 (R-284-000-161-114). M.R.J. acknowledges support from the Biotechnology and Biological Sciences Research Council (BBSRC - project BB/I022570/1) and the BrisSynBio Synthetic Biology Research Centre at the University of Bristol (BB/L01386X/1) funded by the BBSRC and the Engineering and Physical Sciences Research Council (EPSRC) of the UK.

Received: ((will be filled in by the editorial staff))
Revised: ((will be filled in by the editorial staff))
Published online: ((will be filled in by the editorial staff))

References

[1] A. Chortos, J. Liu, Z. Bao, *Nat Mater* **2016**, *15*, 937.
[2] C. Keysers, J. H. Kaas, V. Gazzola, *Nat Rev Neurosci* **2010**, *11*, 417.

[3] D. Gueorguiev, S. Bochereau, A. Mouraux, V. Hayward, J.-L. Thonnard, *Scientific Reports* **2016**, *6*, 25553.
[4] E. A. Lumpkin, M. J. Caterina, *Nature* **2007**, *445*, 858.
[5] R. S. Dahiya, G. Metta, M. Valle, G. Sandini, *IEEE Transactions on Robotics* **2010**, *26*, 1.
[6] M. Krieg, A. R. Dunn, M. B. Goodman, *Nat Cell Biol* **2014**, *16*, 224.
[7] F. McGlone, J. Wessberg, H. Olausson, *Neuron* **2014**, *82*, 737.
[8] H.-H. Chou, A. Nguyen, A. Chortos, J. W. To, C. Lu, J. Mei, T. Kurosawa, W.-G. Bae, J. B.-H. Tok, Z. Bao, *Nature Communications* **2015**, *6*, 8011.
[9] C. Larson, B. Peele, S. Li, S. Robinson, M. Totaro, L. Beccai, B. Mazzolai, R. Shepherd, *Science* **2016**, *351*, 1071.
[10] M. L. Hammock, A. Chortos, B. C. K. Tee, J. B. H. Tok, Z. Bao, *Advanced Materials* **2013**, *25*, 5997.
[11] S. Bauer, S. Bauer-Gogonea, I. Graz, M. Kaltenbrunner, C. Keplinger, R. Schwödiauer, *Advanced Materials* **2014**, *26*, 149.
[12] Z. Zou, C. Zhu, Y. Li, X. Lei, W. Zhang, J. Xiao, *Science Advances* **2018**, *4*, eaaq0508.
[13] X. Pu, M. Liu, X. Chen, J. Sun, C. Du, Y. Zhang, J. Zhai, W. Hu, Z. L. Wang, *Science Advances* **2017**, *3*, e1700015.
[14] Y. Chen, S. Lu, S. Zhang, Y. Li, Z. Qu, Y. Chen, B. Lu, X. Wang, X. Feng, *Science Advances* **2017**, *3*, e1701629.
[15] T. Yokota, P. Zalar, M. Kaltenbrunner, H. Jinno, N. Matsuhisa, H. Kitanosako, Y. Tachibana, W. Yukita, M. Koizumi, T. Someya, *Science Advances* **2016**, *2*, e1501856.
[16] G. S. C. Bermúdez, D. D. Karnaushenko, D. Karnaushenko, A. Lebanov, L. Bischoff, M. Kaltenbrunner, J. Fassbender, O. G. Schmidt, D. Makarov, *Science Advances* **2018**, *4*, eaao2623.
[17] S. C. B. Mannsfeld, B. C. K. Tee, R. M. Stoltenberg, C. V. H. H. Chen, S. Barman, B. V. O. Muir, A. N. Sokolov, C. Reese, Z. Bao, *Nat Mater* **2010**, *9*, 859.
[18] L. Pan, A. Chortos, G. Yu, Y. Wang, S. Isaacson, R. Allen, Y. Shi, R. Dauskardt, Z. Bao, *Nature Communications* **2014**, *5*, 3002.
[19] K. Takei, T. Takahashi, J. C. Ho, H. Ko, A. G. Gillies, P. W. Leu, R. S. Fearing, A. Javey, *Nat Mater* **2010**, *9*, 821.
[20] S.-H. Shin, S. Ji, S. Choi, K.-H. Pyo, B. Wan An, J. Park, J. Kim, J.-Y. Kim, K.-S. Lee, S.-Y. Kwon, J. Heo, B.-G. Park, J.-U. Park, *Nature Communications* **2017**, *8*, 14950.
[21] B. C. K. Tee, C. Wang, R. Allen, Z. Bao, *Nat Nano* **2012**, *7*, 825.
[22] D. J. Lipomi, M. Vosgueritchian, B. C. K. Tee, S. L. Hellstrom, J. A. Lee, C. H. Fox, Z. Bao, *Nat Nano* **2011**, *6*, 788.
[23] G. Schwartz, B. C. K. Tee, J. Mei, A. L. Appleton, D. H. Kim, H. Wang, Z. Bao, *Nature Communications* **2013**, *4*, 1859.
[24] S. Gong, W. Schwalb, Y. Wang, Y. Chen, Y. Tang, J. Si, B. Shirinzadeh, W. Cheng, *Nature Communications* **2014**, *5*, 3132.
[25] X. Wang, Y. Gu, Z. Xiong, Z. Cui, T. Zhang, *Advanced Materials* **2014**, *26*, 1336.
[26] U. Khan, T.-H. Kim, H. Ryu, W. Seung, S.-W. Kim, *Advanced Materials* **2017**, *29*, 1603544.
[27] S. Ma, F. Ribeiro, K. Powell, J. Lutian, C. Møller, T. Large, J. Holbery, *ACS applied materials & interfaces* **2015**, *7*, 21628.
[28] F. Bonaccorso, Z. Sun, T. Hasan, A. C. Ferrari, *Nat Photon* **2010**, *4*, 611.
[29] S. Jung, J. H. Kim, J. Kim, S. Choi, J. Lee, I. Park, T. Hyeon, D.-H. Kim, *Advanced Materials* **2014**, *26*, 4825.
[30] Y. Zang, F. Zhang, D. Huang, X. Gao, C.-a. Di, D. Zhu, *Nature Communications* **2015**, *6*, 6269.

[31] Y. Zhang, Y. Yang, Y. Gu, X. Yan, Q. Liao, P. Li, Z. Zhang, Z. Wang, *Nano Energy* **2015**, *14*, 30.
[32] W. Wu, Z. L. Wang, *Nature Reviews Materials* **2016**, *1*, 16031.
[33] Y. Zhang, X. Yan, Y. Yang, Y. Huang, Q. Liao, J. Qi, *Advanced Materials* **2012**, *24*, 4647.
[34] W. Wu, X. Wen, Z. L. Wang, *Science* **2013**, *340*, 1234855.
[35] F.-R. Fan, L. Lin, G. Zhu, W. Wu, R. Zhang, Z. L. Wang, *Nano Letters* **2012**, *12*, 3109.
[36] T. Quan, X. Wang, Z. L. Wang, Y. Yang, *Acs Nano* **2015**, *9*, 12301.
[37] M. Kaltenbrunner, M. S. White, E. D. Głowacki, T. Sekitani, T. Someya, N. S. Sariciftci, S. Bauer, *Nature Communications* **2012**, *3*, 770.
[38] S. Xu, Y. Zhang, J. Cho, J. Lee, X. Huang, L. Jia, J. A. Fan, Y. Su, J. Su, H. Zhang, H. Cheng, B. Lu, C. Yu, C. Chuang, T.-i. Kim, T. Song, K. Shigeta, S. Kang, C. Dagdeviren, I. Petrov, P. V. Braun, Y. Huang, U. Paik, J. A. Rogers, *Nature Communications* **2013**, *4*, 1543.
[39] Q. Zhang, Q. Liang, Q. Liao, F. Yi, X. Zheng, M. Ma, F. Gao, Y. Zhang, *Advanced Materials* **2017**, *29*, 1606703.
[40] F. R. Fan, W. Tang, Z. L. Wang, *Advanced Materials* **2016**, *28*, 4283.
[41] Z. L. Wang, *Acs Nano* **2013**, *7*, 9533.
[42] Z. L. Wang, W. Wu, *Angewandte Chemie International Edition* **2012**, *51*, 11700.
[43] J. Kim, M. Lee, H. J. Shim, R. Ghaffari, H. R. Cho, D. Son, Y. H. Jung, M. Soh, C. Choi, S. Jung, K. Chu, D. Jeon, S.-T. Lee, J. H. Kim, S. H. Choi, T. Hyeon, D.-H. Kim, *Nature Communications* **2014**, *5*, 5747.
[44] C. Wang, D. Hwang, Z. Yu, K. Takei, J. Park, T. Chen, B. Ma, A. Javey, *Nat Mater* **2013**, *12*, 899.
[45] J. Cadet, E. Sage, T. Douki, *Mutation Research/Fundamental and Molecular Mechanisms of Mutagenesis* **2005**, *571*, 3.
[46] Y. Matsumura, H. N. Ananthaswamy, *Toxicology and Applied Pharmacology* **2004**, *195*, 298.
[47] B. K. Armstrong, A. Kricker, *Journal of Photochemistry and Photobiology B: Biology* **2001**, *63*, 8.
[48] A. Kammeyer, R. M. Luiten, *Ageing Research Reviews* **2015**, *21*, 16.
[49] S. K. Ravi, D. J. Swainsbury, V. K. Singh, Y. K. Ngeow, M. R. Jones, S. C. Tan, *Advanced Materials* **2018**, *30*, 1704073.
[50] V. K. Singh, S. K. Ravi, J. W. Ho, J. K. C. Wong, M. R. Jones, S. C. Tan, *Advanced Functional Materials* **2017**, 1703689.
[51] A. Abouimrane, I. Belharouak, Y. A. Abu-Lebdeh, *Frontiers in Energy Research* **2015**, *3*, 34.
[52] J. E. Fitzpatrick, J. G. Morelli, *Dermatology Secrets Plus E-Book*, Elsevier Health Sciences, **2015**.
[53] E. C. De Fabo, F. P. Noonan, T. Fears, G. Merlino, *Cancer Research* **2004**, *64*, 6372.
[54] V. I. Godik, R. E. Blankenship, T. P. Causgrove, N. Woodbury, *FEBS Letters* **1993**, *321*, 229.
[55] B. Nie, R. Li, J. D. Brandt, T. Pan, *Lab on a Chip* **2014**, *14*, 1107.
[56] J. C. Yeo, J. Yu, M. Shang, K. P. Loh, C. T. Lim, *Small* **2016**, *12*, 1593.
[57] J. C. Yeo, J. Yu, K. P. Loh, Z. Wang, C. T. Lim, *ACS Sensors* **2016**, *1*, 543.

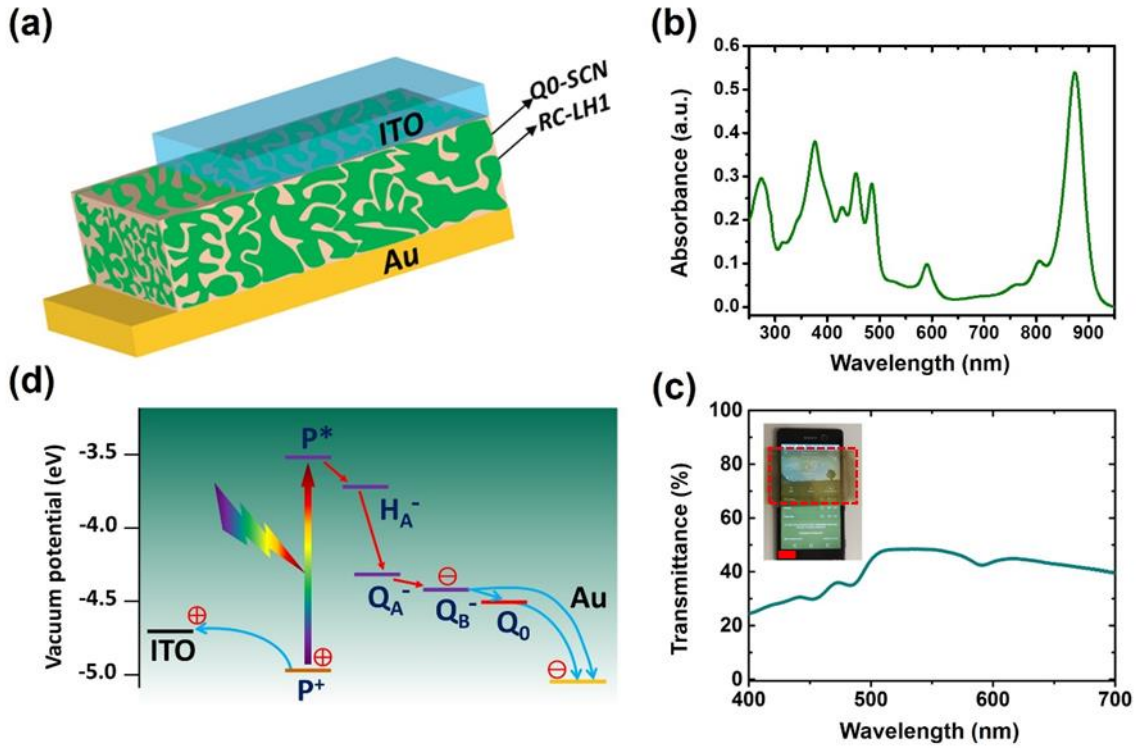

Figure 1. Device architecture, optical properties and mechanism. a**)** Device architecture (ITO-PET/RC-LH1/Q0-SCN/Au-PET). b**)** Absorption spectrum of the RC-LH1 pigment-protein in solution. c) Transmittance of the device across the visible spectrum, inset: image of a section of device (under red dotted-line) covering a mobile phone screen to illustrate transparency; Scale bar: 2 cm. d) Energy diagram showing how photoexcitation of the RC-LH1 complex (rainbow arrow) elicits an intra-protein charge separation (red arrows) and direct or Q0-mediated charge transport to the electrodes (cyan arrows).

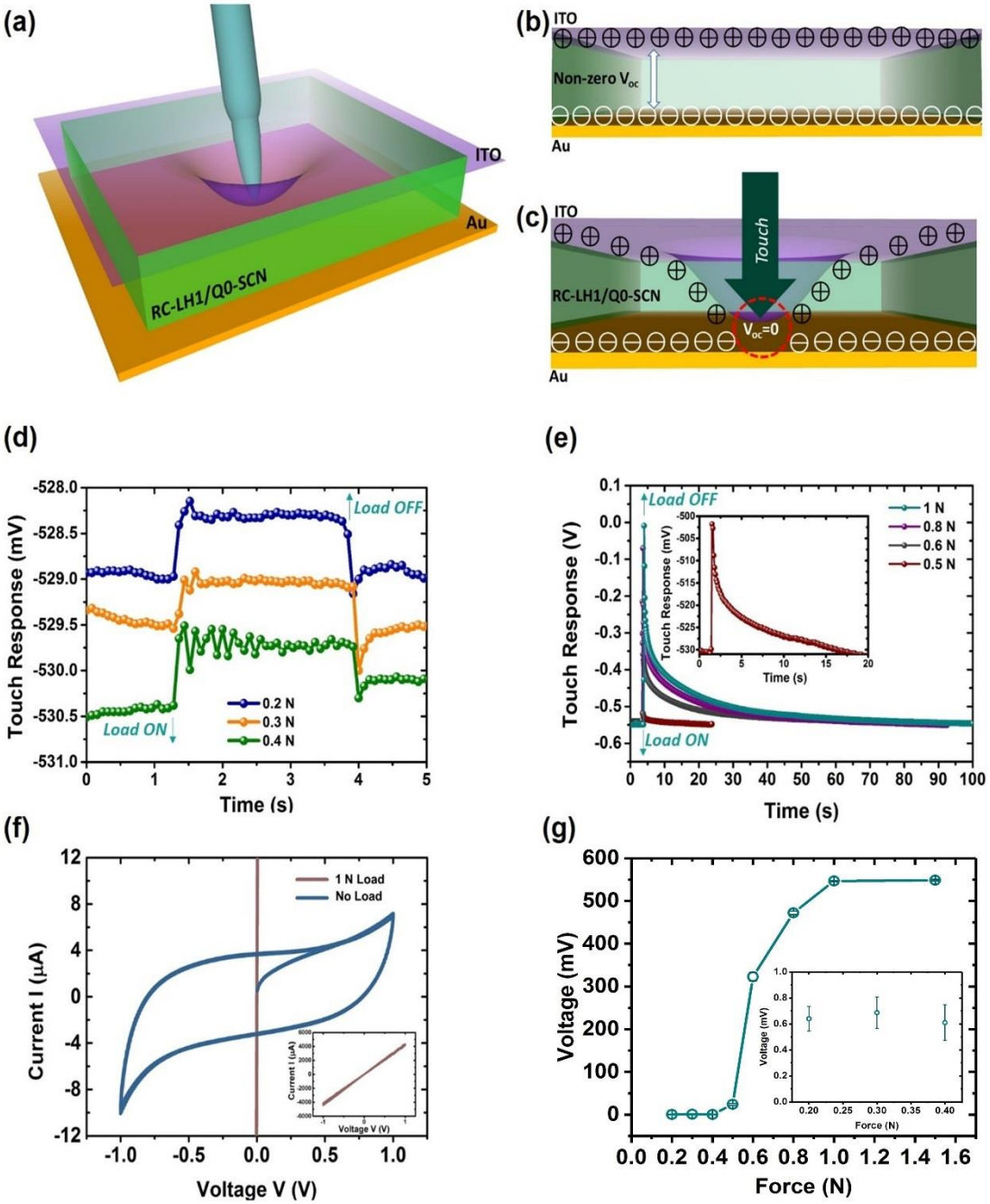

Figure 2. Touch sensing. a) Touch sensing is based on deformation of the top electrode and the protein/Q0-SCN blend. b) The blend supports a V_{OC} between the PET-ITO and PET-Au electrodes. c) The V_{OC} drops to zero in response to a touch that brings the electrodes into contact. d) Voltage changes in response to the application and removal of a 0.2-0.4 N continuous load. e) Voltage changes in response to instantaneous loads of 0.5-1 N. f) IV characteristics showing a drop in resistance on application of a 1 N load. g) Force dependence of the voltage response. Beyond 1 N load, there was no further increase in the voltage response. The area to which the load was applied was 0.6 cm^2, from which the corresponding pressures were calculated.

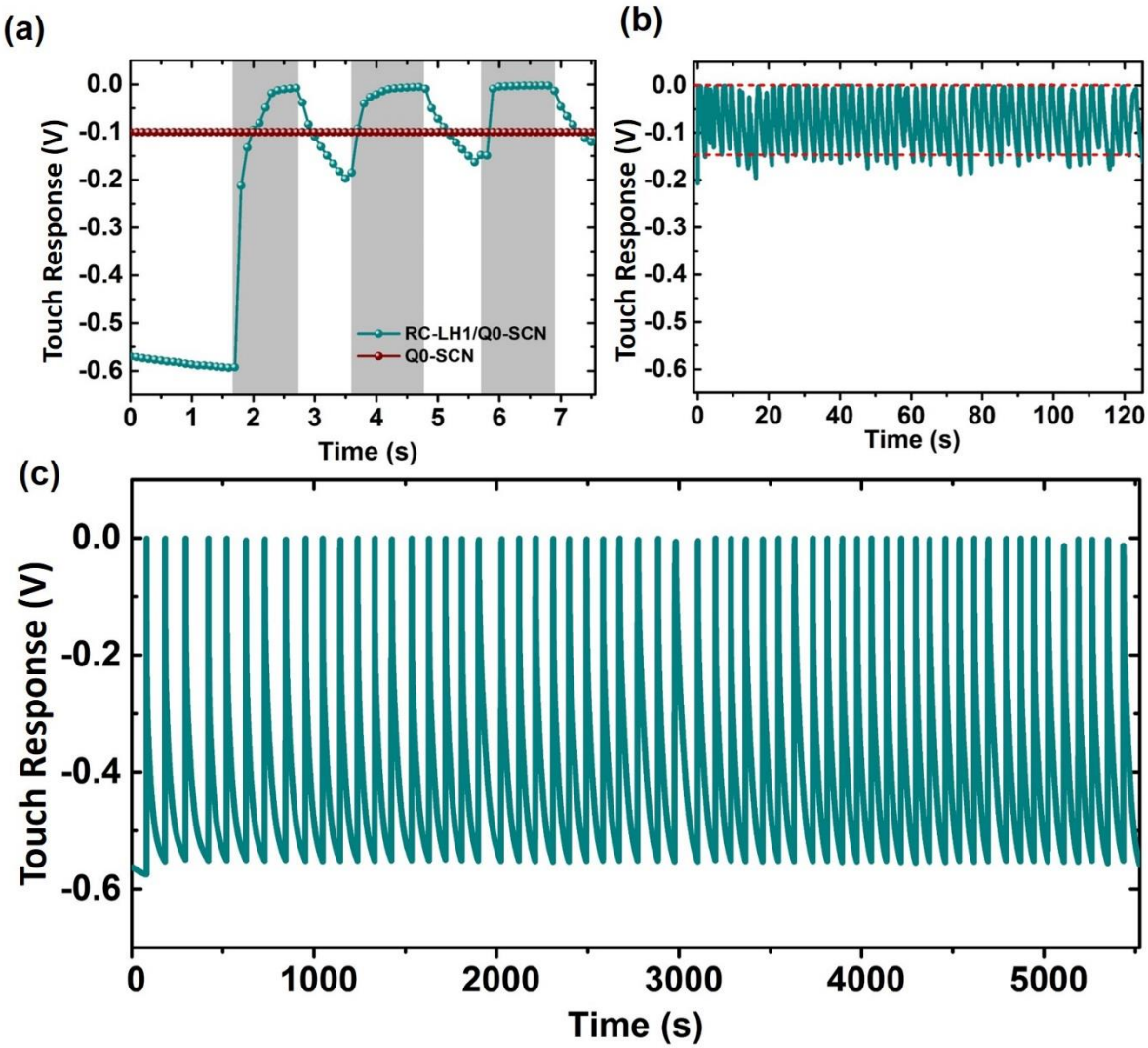

Figure 3. Voltage responses to repetitive touches. a) Utilization of a 0.1 V touch response to achieve a reaction time of < 1 s, the voltage returning to -0.1 V from zero within 1 s of the removal of load. b) Repeatability of the loading/unloading response over multiple cycles initiated after a voltage of -0.15 V was reached. c) Repeatability of the loading/unloading response over multiple cycles initiated after the voltage reached the baseline (-0.57 V).

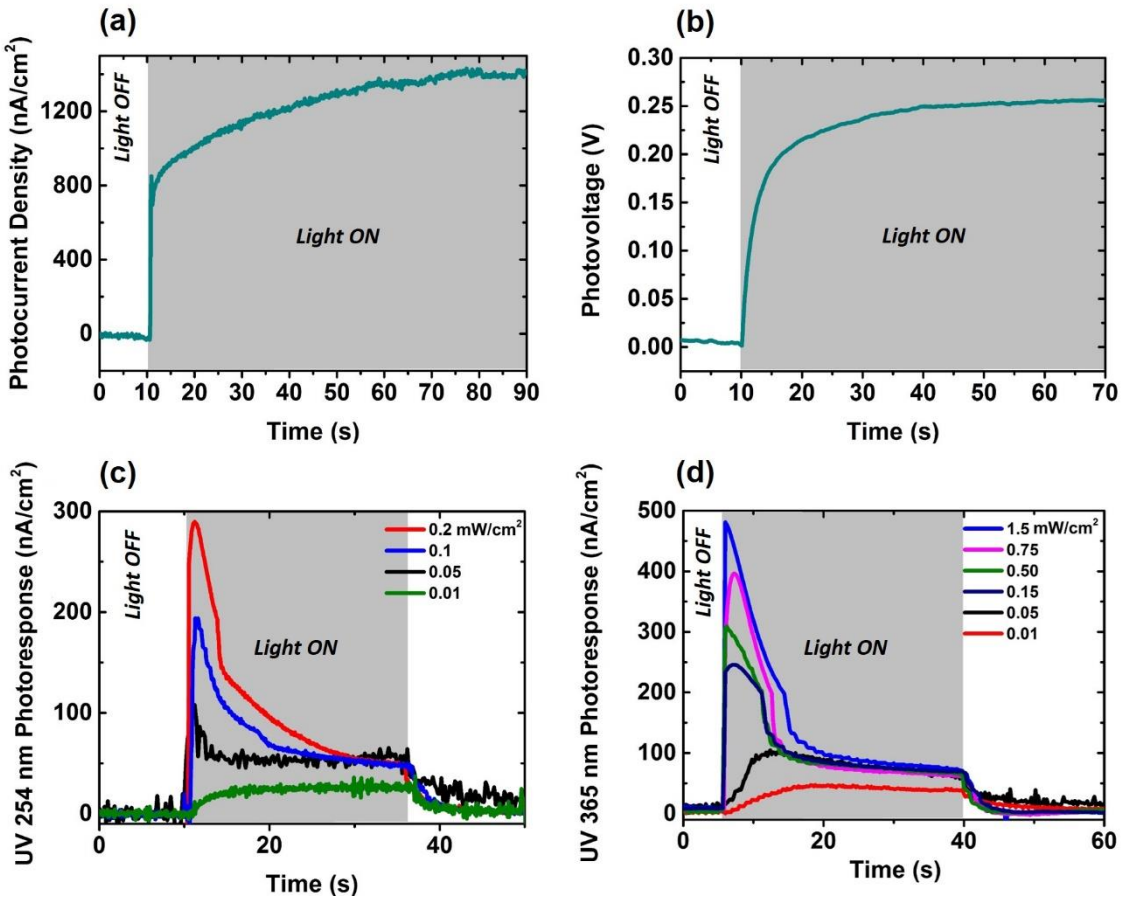

Figure 4. Solar energy conversion and UV sensing. a) Photocurrent density and b) Photovoltage in response to white light excitation. c) Photocurrent density in response to 254 nm excitation. d) Photocurrent density in response to 365 nm excitation.

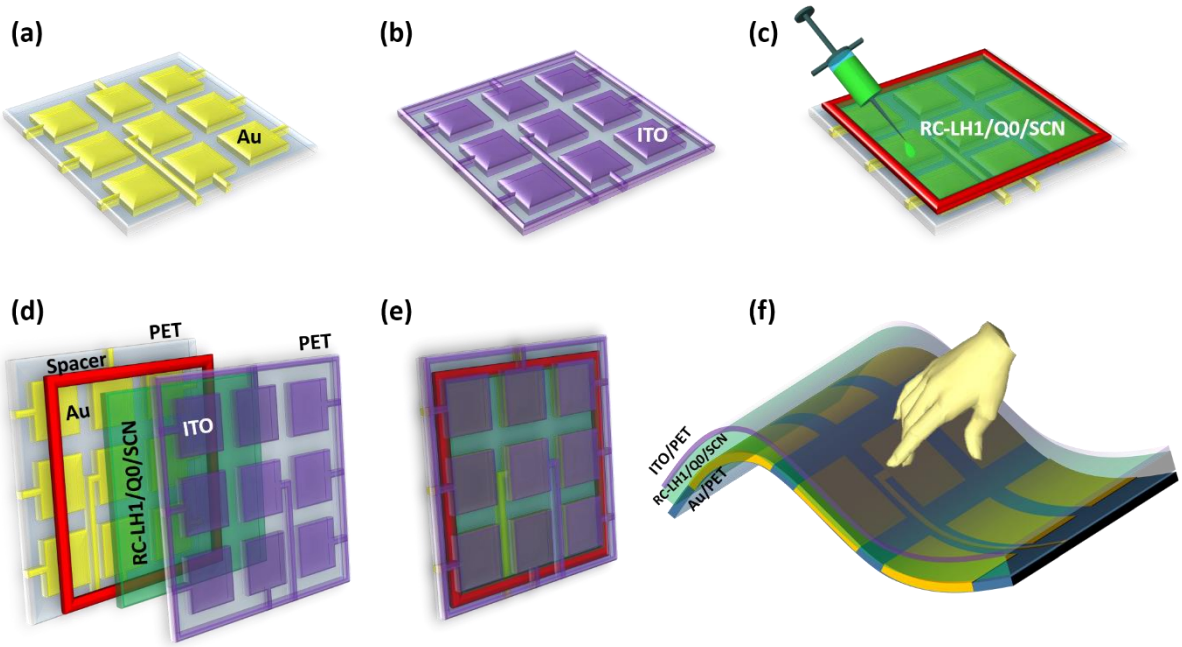

Figure 5. Construction of a multi-pixel sensor. a) Deposition of Au or, b) ITO in nine pixels on PET substrates. c) Coverage of the Au-PET substrate protein/Q0-SCN blend within the boundary of a peripheral spacer. d) Sandwiching of the protein/Q0-SCN blend between the electrodes. e) Final device architecture with the nine Au pixels connected to separate terminals and the nine ITO pixels connected to a common terminal. f) Assessment of touch and tracking responses from the flexible multi-pixel sensor.

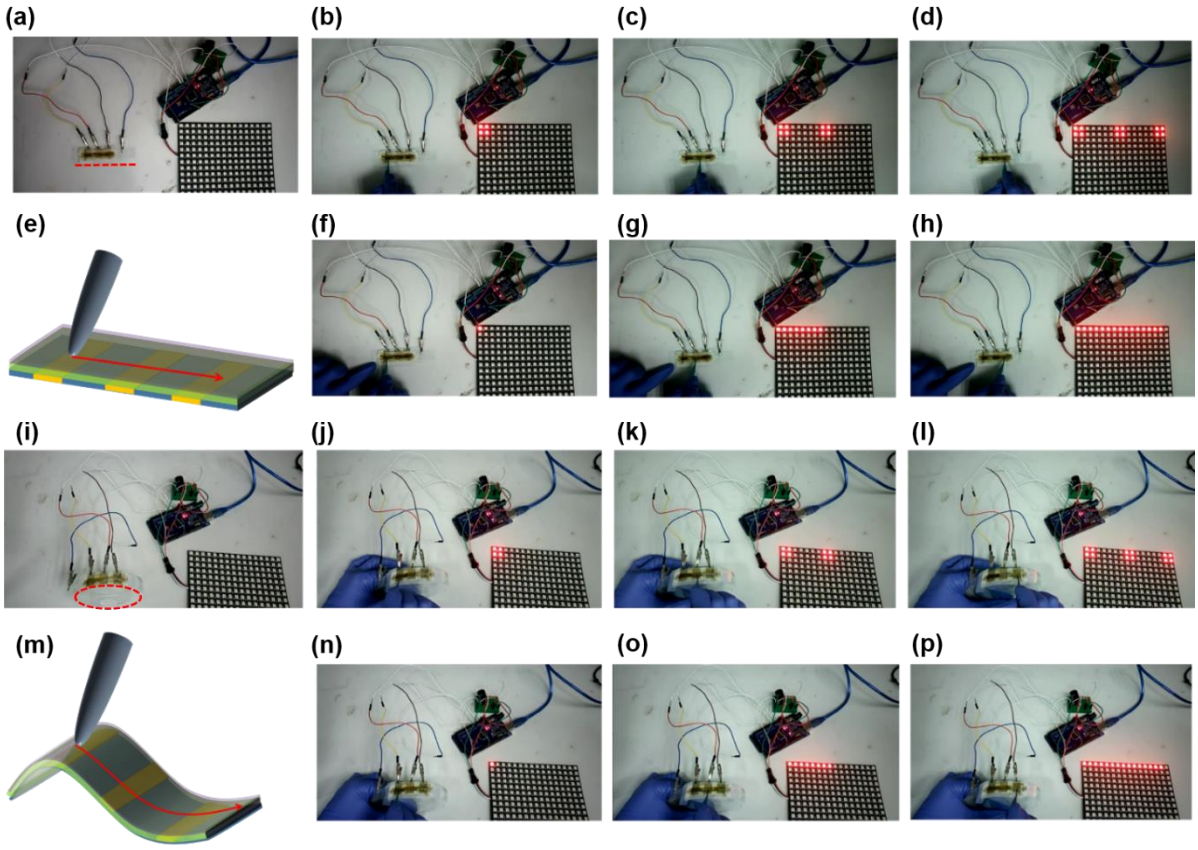

Figure 6. Touch registration and tracking by a 3-pixel sensor connected to an LED readout. a-d) Touch registration on a flat surface before touching (a) and after touching the (left to right) first (b), second (c) and third pixel (d). e-h) Touch tracking on a flat surface (e) by moving a stylus continuously left to right from pixel 1 (f) over pixel 2 (g) to pixel 3 (h). i-l) Touch registration with the 3-pixel sensor flexed over the rim of a petri dish (highlighted by the red dashed ellipse in (i)). m-p) touch tracking using the same curved 3-pixel sensor.

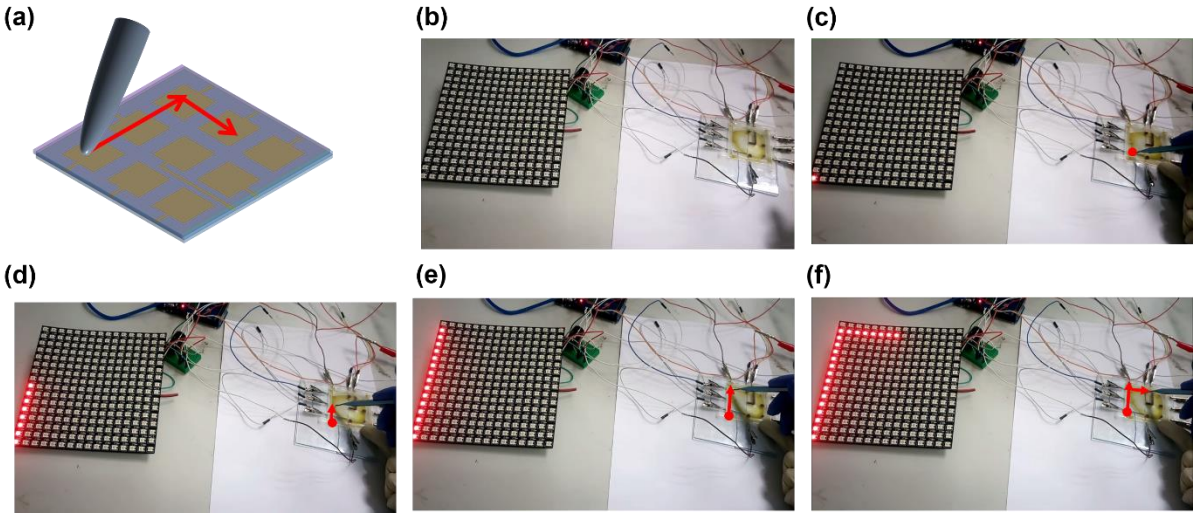

Figure 7. Touch tracking using a 9-pixel sensor connected to an LED readout. a) Schematic of a touch stimulus moving continuously along the multi-pixel sensor. b-f) Touch tracking before (b) and during (c-f) tracing an L-shape on the 9-pixel sensor.

Towards a self-powered photosynthetic electronic skin, a bioelectronic sensor has been developed that makes use of natural photosynthetic pigment-protein complexes to sustain a variety of functions including touch-perception, UV-detection and nanopower generation. Touch responses can be elicited by a variety of natural or synthetic materials, and touch can be sensed under water and in the dark. Proof-of-concept multipixel devices are shown to be capable of touch registration and tracking, and applications such as UV sensing e-skins are considered.

Keyword: Polysensory e-skin, Tactile sensing, Electronic skin, Flexible electronics, Photosynthetic proteins, Nanopower generation, Energy Self-sufficiency

*Sai Kishore Ravi, Tingfeng Wu, Vishnu Saran Udayagiri, Xuan Minh Vu, Yanan Wang, Michael R. Jones, Swee Ching Tan**

Photosynthetic Bioelectronic Sensors for Touch Perception, UV-Detection and Nanopower Generation: Toward self-powered e-skins

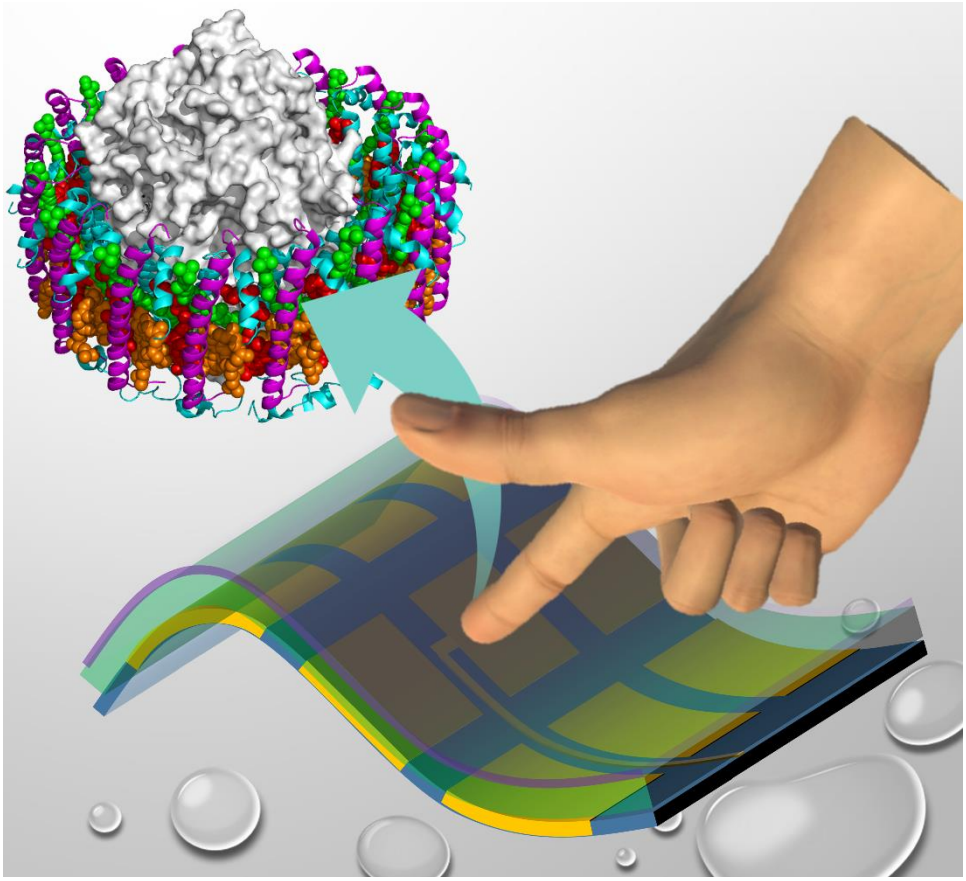

Supporting Information

Photosynthetic Bioelectronic Sensors for Touch Perception, UV-Detection and Nanopower Generation: Toward self-powered e-skins

*Sai Kishore Ravi, Tingfeng Wu, Vishnu Saran Udayagiri, Xuan Minh Vu, Yanan Wang, Michael R. Jones, Swee Ching Tan**

Experimental Section

The bioelectronic sensor was fabricated by using a flexible top electrode comprising an indium tin oxide coated polyethylene terephthalate film (ITO-PET) and a gold-PET base electrode separated by a blend of photosynthetic protein and electron transfer mediator in a gap maintained by a double sided adhesive spacer (≈250 μm thick). The ITO (≈200 nm thick) and gold films (≈20 nm thick) were deposited by magnetron sputtering, using a mask to produce multiple pixels with independent or common terminals. *Rhodobacter sphaeroides* RC-LH1 reaction centre/light harvesting complexes lacking the PufX protein and with green carotenoids were purified as described previously [**S1, S2**]. The mediator was 100 mM ubiquinone-0 (Q0) dispersed in a gel matrix formed from succinonitrile (SCN) and water mixed in a 40:1 ratio (v/v). Solutions of concentrated protein (100 μM) and Q0-SCN were mixed in a 5:1 ratio (v/v) to form a two-phase system. The absorbance of the protein solution and the transmittance of the device were measured using a Shimadzu UV-Vis spectrophotometer. Voltage responses to touch, photovoltages and photocurrents were measured using an Autolab electrochemical workstation (Metrohm). Photo-excitation was provided using UV light (254 nm and 365 nm) or white light (100 mW/cm^2). The different UV light intensities were achieved by varying the distance between the sample and the light source and the intensities were measured using a Si photodetector. Using two UV light sources, one of wavelength 254 nm and the other of 365 nm, at each intensity, a photocurrent was recorded in a Light OFF/Light ON/Light OFF cycle using

a Keithley K2400 sourcemeter. For visualisation of touch responses by multi-pixel devices an electronic microcontroller interface was used to translate the voltage signals from the touch sensor to illumination of an LED array. In the circuit, the Au electrodes of the multiple pixels were connected to analogue input pins on the microcontroller board while the ITO electrodes were connected to ground. The microcontroller's on-board analogue-to-digital converter was used to read in the voltages generated by each pixel and the data were recorded. A 5-volt WS2812 16-by-16 multicolour LED array panel was connected to the microcontroller for data visualisation. In case of the 9-pixel sensor, the LED array was divided into nine segments, where each segment depicted the voltage status of each pixel.

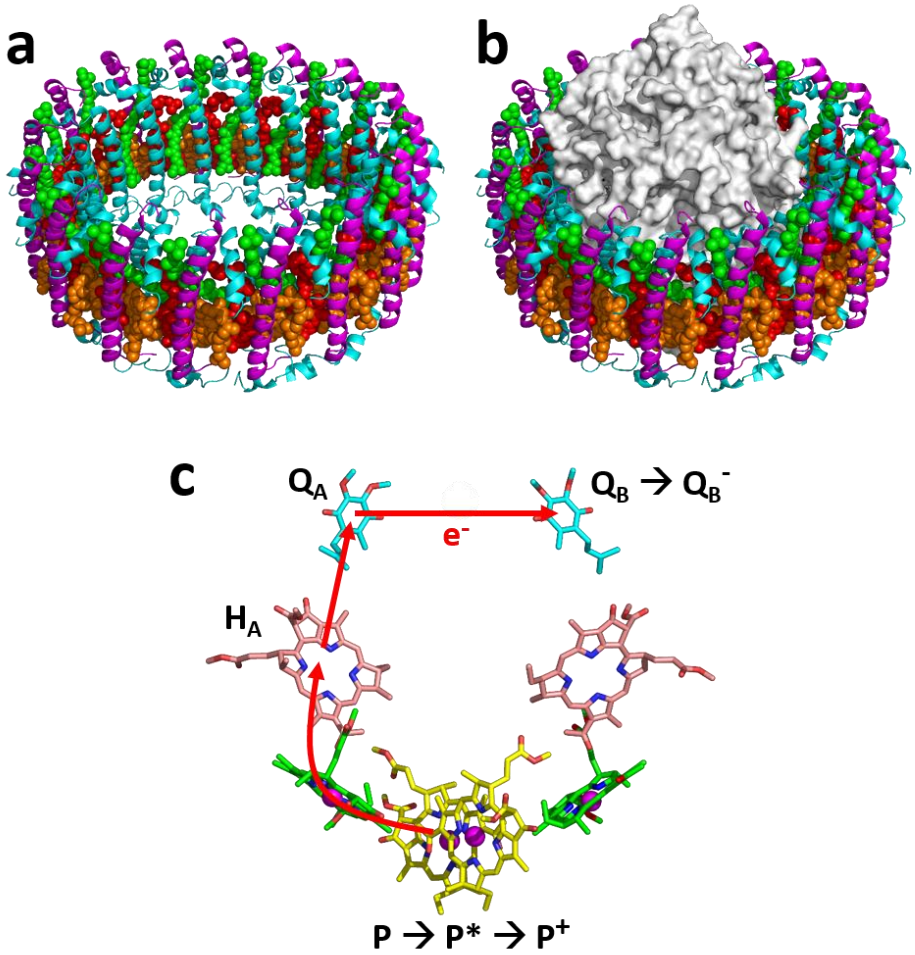

Figure S1. Structure of the RC-LH1 complex and the mechanism of photochemical charge separation. A guide to the structure of the membrane-embedded PufX-deficient RC-LH1 pigment-protein complex from *Rba. sphaeroides* is provided by a 3.0 Å resolution X-ray crystal structure for the related RC-LH1 complex from the bacterium *Thermochromatium tepidum* [**S3**]. a) View of the LH1 component at an angle of approximately 45° to the plane of the membrane. It comprises concentric cylinders of 16 α-polypeptides (cyan ribbons) and 16 β-polypeptides (magenta ribbons). These hold in place a ring of 32 bacteriochlorophylls (alternating red and orange spheres) and a ring of 16 carotenoids (green spheres). The *Rba. sphaeroides* RC-LH1 contains an additional ring of 16 carotenoids. b) The RC component (white surface) occupies the space at the centre of the LH1 cylinder and comprises three polypeptides. c) Arrangement of electron transfer cofactors within the RC. They comprise four bacteriochlorophylls (magenta sphere denotes central Mg atom), two of which (yellow carbons) from an excitonically-coupled pair (P). Charge separation involves transfer of an electron from the first singlet excited state of P (P*) to a bacteriopheophytin acceptor (H_A - pink carbons) via a monomeric bacteriochlorophyll (green carbons). The electron is then passed on to an immobile ubiquinone-10 (Q_A – cyan carbons) and then to a dissociable ubiquinone-10 (Q_B). The result is a membrane-spanning radical pair $P^+Q_B^-$ that in RC-LH1 complexes has a recombination lifetime of several seconds. All of the bacteriochlorophyll, bacteriopheophytin and carotenoid pigments of the RC-LH1 complex act as light harvesting pigments, transferring excited state energy to the P bacteriochlorophylls to initiate charge separation.

Model for UV-Sensing and Discrimination

Exploiting the UV-absorbing property of the RC-LH1 proteins, and the associated photocurrent (**Figure S2a**), a proof-of-concept model is proposed that has the ability both to sense light intensity and indicate the category of UV light. This can be achieved by simply incorporating three different optical filters on a multipixel device as shown in **Figure S2b**. By covering part of the device with a short-pass filter that blocks all wavelengths greater than 300 nm, the pixels under this filter produce a response specific to short-wave exposure. Likewise a 300-400 nm bandpass filter could be used to produce an area specific to longwave UV. In normal sunlight, exposure to safe conditions would be indicated by the inactivity of pixels under the short-pass and the band-pass filters, with only the pixels under the >400 nm long-pass filter being functional. This response could be digitized as a 0 0 1 state to notify that there is no short-wave or long-wave UV light in the incident sunlight (**Figure S2c**). Similarly 0 1 1 and 1 1 1 states would notify on the presence of long-wave UV or both short- and long-wave UV, respectively (Fig. S2c). This model could further be improved to notify both the category of UV light and its intensity.

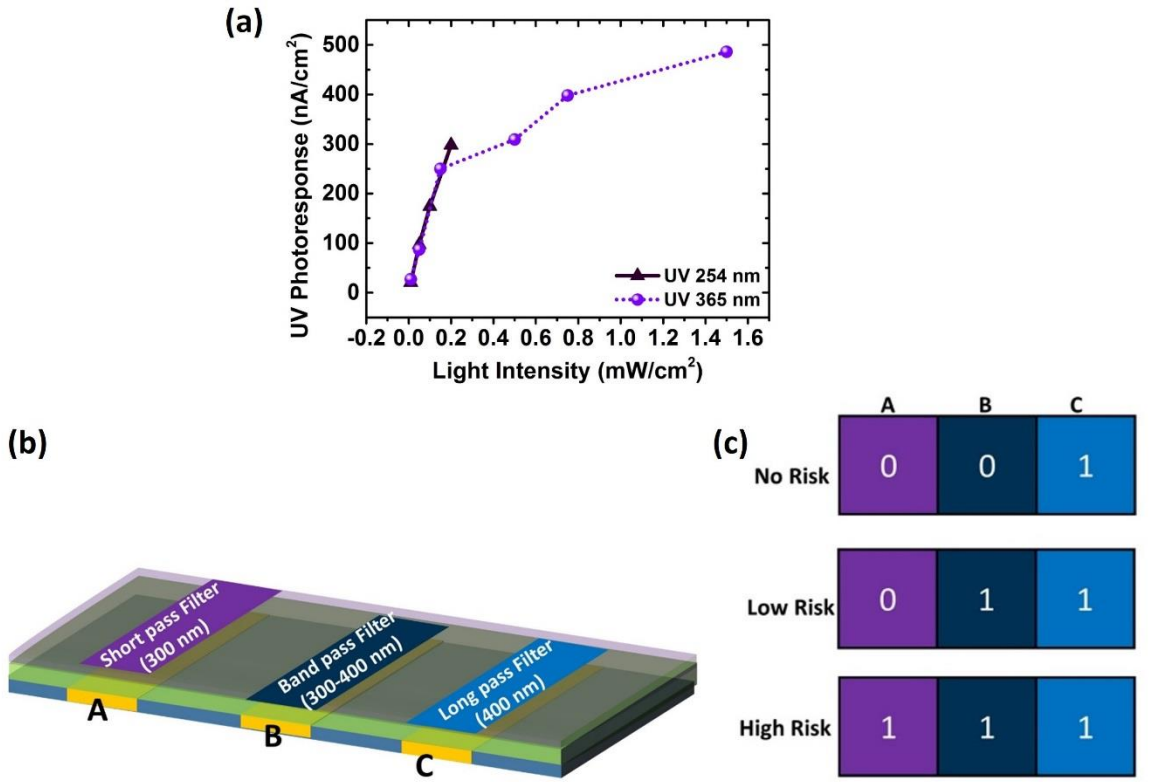

Figure S2. Model of a UV-sensing device. a) Dependence of the UV photoresponse on light intensity. b) Model of device to distinguish different wavelengths with optical filters placed over separate pixels (A-C). c) Device output to identify different UV risks.

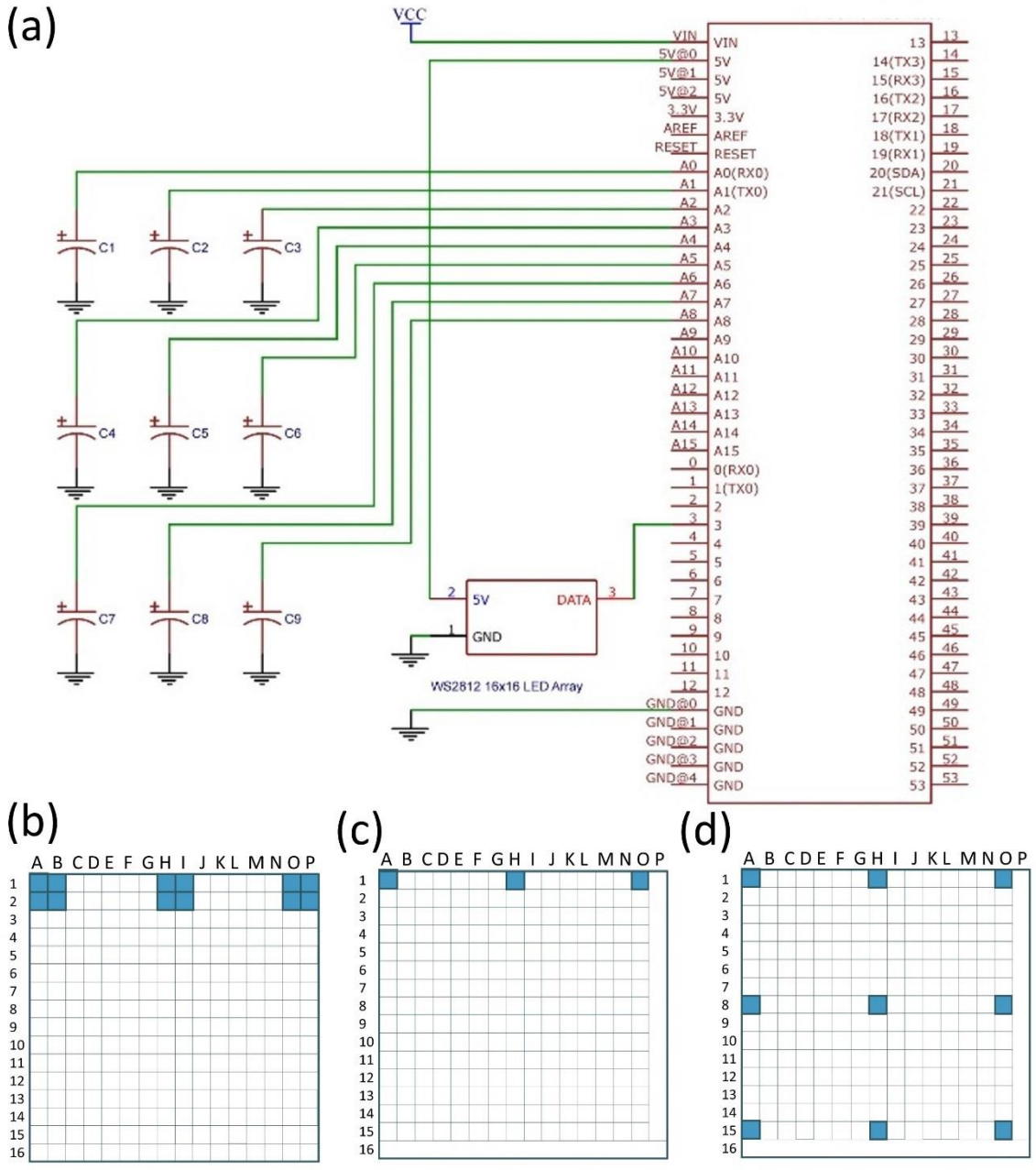

Figure S3. Electronic interface used to translate voltage signals from the a 9-pixel touch sensor to an LED array. a) Each pixel in the 9-pixel device is represented by an electrochemical capacitor (C1 to C9). The Au electrodes of each of the nine pixels are connected to analog input pins A0-A8 on a microcontroller board and the ITO electrodes are connected to ground. The microcontroller's on-board analog-to-digital converter read in the voltages from each pixel and the data are recorded. A 5-volt WS2812 16-by-16 multicolour LED array panel was also connected to the microcontroller. b) In the case of touch registering using a 3-pixel device, the signal from each pixel is translated to a block of four LEDs in the 16-by-16 array. Each LED in the array is identified by its column letter (A to P) followed by row number (1 to 16). Pixel 1 in the sensor corresponds to A1-B1-A2-B2, pixel 2 to H1-I1-H2-I2, pixel 3 to O1-P1-O2-P2. c) In touch-tracing in the 3-pixel device, pixel 1 corresponds to A1, pixel 2 to H1 and pixel 3 to O1. d) For touch-tracing in the 9-pixel device, the signals from pixels 1 to 9 is translated to

the LED array as follows: 1→A1, 2→H1, 3→O1, 4→A8, 5→H8, 6→O8, 7→A15, 8→H15, 9→O15.

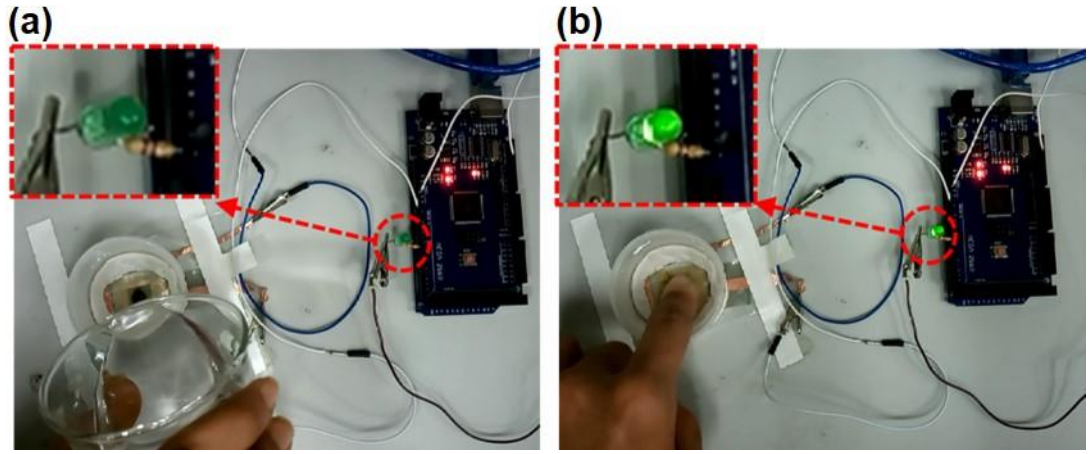

Figure S4. Touch responses under water. a) Overlaying the sensor with water does not produce a response. b) A finger can elicit a touch response under water (Refer to **Movie S1**).

On the Touch Sensing Function.

All of the touch sensing demonstrations carried out essentially rely on the built-in base voltage in the device, and so were independent of any external illumination (see **Movie S2**). Given a constant built-in potential and a constant resistivity of the protein-electrolyte matrix between the two electrodes, it is known that the resistance of a section decreases with decreasing section length (i.e. the distance between the electrodes). Under no applied pressure (i.e. before touch), there are no resistance changes anywhere in the device as the electrode-separation distance is unchanged. Under pressure (i.e. upon touch), a local zone is formed where the electrode separation distance is lowered, hence creating a path of relatively lower resistance. Under sufficient pressure, the two electrodes come into direct contact reducing the separation distance in that local zone to zero. This generates a sharp shift in voltage as the resistance in that zone drops to zero. Though the overall tactile sensing mechanism may be different, the formation of a low resistance zone upon pressure application is similar to the device-level or material-level resistance changes in resistive sensors [**S4, S5**]. This touch response in the device should not to be confused with any pressure-induced voltage fluctuation in a solar cell. Touch-induced voltage changes in flexible solar cells are typically minor and occur only under illumination as the base voltage in dark would be near-zero. However, in this bioelectronic sensor, the voltage responses to touch are observed without any use of illumination. For convenience, all the demonstrations (**Movies S1 and S3 to S7**) are shown under ambient light conditions in the laboratory, the intensity of which did not exceed 0.1 mW/cm^2, which is 1000 times lower than the standard illumination intensity (1 Sun) used for a solar cell. The base voltage of the device was essentially the same both in the dark (0 mW/cm^2) and under the ambient room light (0.1 mW/cm^2). This implies that the touch sensing ability of the device remains functional even in the dark. For confirmation, an additional demonstration has been presented (**Movie S2**) that shows the touch sensing capability of the bioelectronic sensor covered by a black cloth, making the light intensity reaching the device surface zero.

Supplementary Movies

Movie S1 Demonstration of touch sensing in air and under water

Movie S2 Demonstration of touch sensing in the dark

Movie S3 Demonstration of touch registration by a 3-pixel sensor on a flat surface

Movie S4 Demonstration of touch tracking by a 3-pixel sensor on a flat surface

Movie S5 Demonstration of touch registration by a 3-pixel sensor on a curved surface

Movie S6 Demonstration of touch tracking by a 3-pixel sensor on a curved surface

Movie S7 Demonstration of touch tracking by a 9-pixel sensor on a flat surface

Supplementary References:

S1 Ravi, S.K., Yu, Z., Swainsbury, D.J., Ouyang, J., Jones, M.R. and Tan, S.C. Enhanced output from biohybrid photoelectrochemical transparent tandem cells integrating photosynthetic proteins genetically modified for expanded solar energy harvesting. *Adv. Energy Mater.* **7**, 1601821 (2017).

S2 Friebe, V.M., Delgado, J.D., Swainsbury, D.J.K., Gruber, J.M., Chanaewa, A., van Grondelle, R., von Hauff, E., Millo, D., Jones, M.R. and Frese, R.N. Plasmon-enhanced photocurrent of photosynthetic pigment proteins on nanoporous silver. *Adv. Funct. Mater.* **26**, 285 (2016).

S3 Niwa, S., Yu, L.-J., Takeda, K., Hirano, Y., Kawakami, T., Wang-Otomo, Z.-Y. and Miki, K., Structure of the LH1-RC complex from *Thermochromatium tepidum* at 3.0 Å. *Nature* **508**, 228 (2014).

S4 Zhang, H. and So, E., Hybrid resistive tactile sensing. *IEEE Transactions on Systems, Man, and Cybernetics, Part B (Cybernetics)*, **32**, 57 (2002).

S5 Pan, L., Chortos, A., Yu, G., Wang, Y., Isaacson, S., Allen, R., Shi, Y., Dauskardt, R. and Bao, Z., An ultra-sensitive resistive pressure sensor based on hollow-sphere microstructure induced elasticity in conducting polymer film. *Nat. Commun.* **5**, 3002 (2014).